Supplement of Atmos. Meas. Tech., 13, 4317–4331, 2020
https://doi.org/10.5194/amt-13-4317-2020-supplement

Atmospheric
Measurement
Techniques
Open Access

Supplement of

A compact incoherent broadband cavity-enhanced absorption spectrometer for trace detection of nitrogen oxides, iodine oxide and glyoxal at levels below parts per billion for field applications

Albane Barbero et al.

Correspondence to: Roberto Grilli (roberto.grilli@cnrs.fr)

S1 Method

S1.1 Solidworks simulation

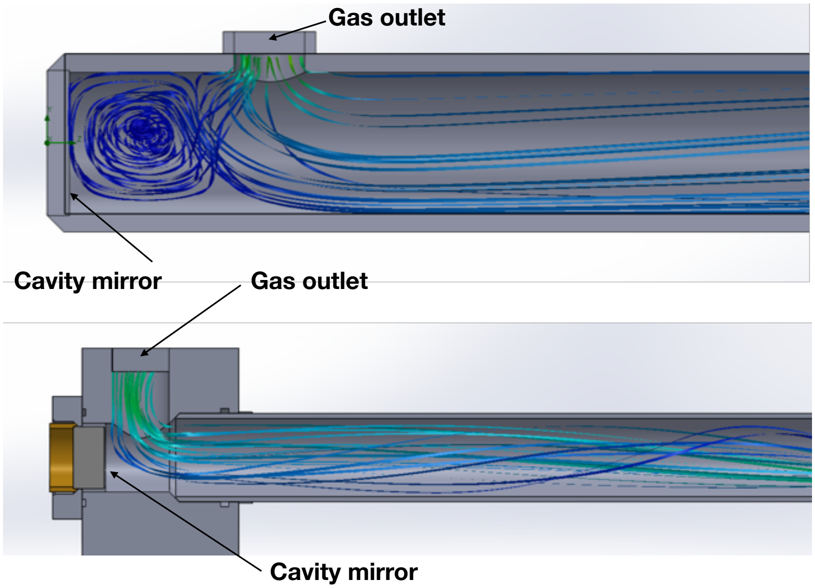

Figure S1. SolidWorks simulations of the air flow entering the cavity at 1 L min^{-1}. **(top)** Turbulences created by the presence of a dead-volume between the cavity mirror and the gas exhaust. **(bottom)** Configuration with an optimum distance between the high reflective mirror and the gas outlet which maximize the effective optical pathlength, avoiding the use of purging gas at the mirrors while preserving the mirrors cleanliness during the measurement. The gas inlet is placed at the center of the cavity.

Solid works simulations were made with two different mirrors positions without purge flow (Fig. S1). With the cavity mirrors placed one or two centimeters away from the exit of the air flow, presence of turbulences in front of the mirrors can be observed, which may compromise the long term cleanliness of the high reflectivity mirrors, Fig. S1 (top). By placing the mirrors close to the gas flow exit, the absence of dead-volume minimizes the residence time of particles by avoiding localized turbulences to take place as shown in Fig. S1 (bottom) and prevents the mirrors surface from deposition of dust and organic matter. In addition, PTFE membrane filters (Whatman® PTFE membrane filters – TE 38, 5 μm, 47 mm) placed at the entrance of each sampling lines, reference and sample, prevent particles to enter the gas lines.

S1.2 Mirrors cleanliness monitoring

A photodiode was mounted on a cap placed in front of the LED assemble. This allow to continuously monitor the LED intensity as $\mathrm{PD_{meas}}$. After a calibration with a standard gas, the value at the photodiode and the mean light intensity at the CCD, while flushing with zero air and averaged over all the pixels, are stored as $\mathrm{PD_{calibr}}$ and $\mathrm{I_{0-calibr}}$, respectively. At any time, the expected intensity, $\mathrm{I_{0-expected}}$, at the CCD can be calculated as follow:

$$\mathrm{I_{0-expected}} = \mathrm{I_{0-calibr}} \left(\frac{\mathrm{PD_{meas}}}{\mathrm{PD_{calibr}}} \right) \quad (1)$$

and compare to the intensity at the CCD during measurements, $I_{0-\mathrm{meas}}$. The ratio $I_{0-\mathrm{meas}}$ / $I_{0-\mathrm{expected}}$ is therefore a direct indicator of the mirrors cleanliness as the variability of the LED intensity is accounted for in real time. Fig. S2 shows a timeseries of 10 days measurements during which no calibrations were made. The variability of the LED intensity, Fig. S2(a), is less than 0.05 % over 10 continuous days, implying that the variability of the signal intensity, Fig. S2(b), only represents the mirror cleanliness over time. The variability of the latter, being less than 2 % (3 σ), validates the stability of the mirror reflectivity over time with the described set-up of our instruments and without purge flow.

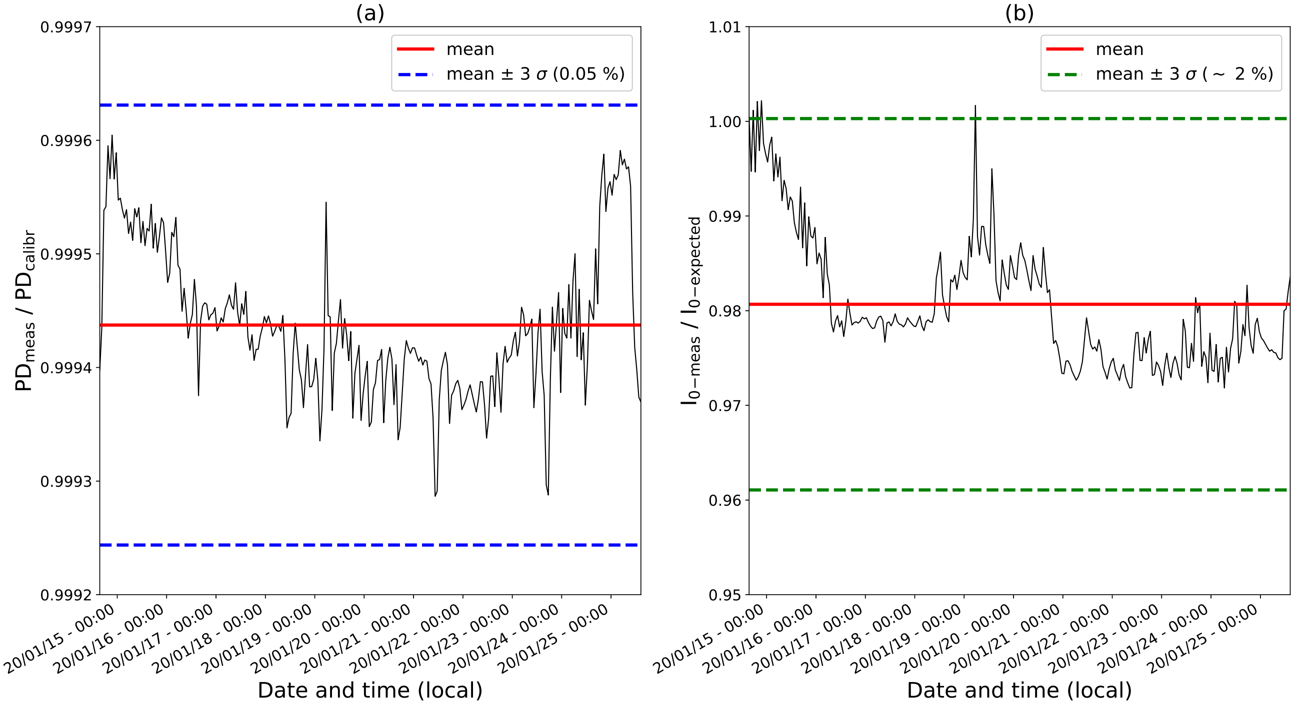

Figure S2. Monitored signals over 10 continuous days of measurement without any adjustment or calibration of the instrument. **(a)** $\mathrm{PD}_{\mathbf{meas}}$ / $\mathrm{PD}_{\mathbf{calibr}}$ and **(b)** $I_{0-\mathbf{meas}}$ / $I_{0-\mathbf{expected}}$.

S2 Spectral Fit

For retrieving the wavelength dependent mirror reflectivity curve, literature spectrum from Vandaele et al. (1998) was convoluted by the known instrumental function of the spectrometer (18 cm^{-1} Lorentzian broadening). The convoluted literature spectrum is then transformed into absorption coefficient for given NO_2 and CHOCHO concentrations, in this case 49.6 and 32.7 ppb, respectively, by using the combination of equations 1 and 2 reported in the manuscript. It should be noticed that the trace gas concentration only plays on the mirror reflectivity curve offset and is not critical for determining its shape. As a first guess for the reflectivity curve, the theoretical values provided by the mirror manufacturer were use. The polynomial coefficients used to describe the mirror reflectivity curve were then slightly adjusted to achieve the best match between the convoluted literature spectrum and the measured spectrum (i.e. lower root-mean-square on the difference between the two data sets). This was done for NO_2, for which the concentration was known since delivered by the Kin-Tek calibrator. The shape of the curve was then confirmed by comparing another experimental spectrum of CHOCHO with its litterature cross-sections (convoluted with the same convolution function). In the Fig. S3 (top) the optimal mirror reflectivity curve is reported, together with the theoretical curve provided by the manufacturer. Fig. S3 (middle) and (bottom) show the convoluted (black)and unconvoluted (grey) literature spectra from Vandaele et al. (1998) for NO_2 and Volkamer et al. (2005) for CHOCHO, in unit of absorption coefficient, together with the acquired IBBCEAS spectra (red). The blue lines represent the difference between the experimental and the convoluted literature spectra. Small discrepancies are visible which could be due to small anomalies in the mirror reflectivity curve or to some experimental bias either on the literature or the IBBCEAS spectra (i.e. an inhomogeneous response of the pixels of the CCD camera or a bad baseline subtraction). Nevertheless, this does not represent an issue here since the references spectra used for the fit analysis are the ones experimentally acquired by the same IBBCEAS instrument and calibrated against literature cross sections.

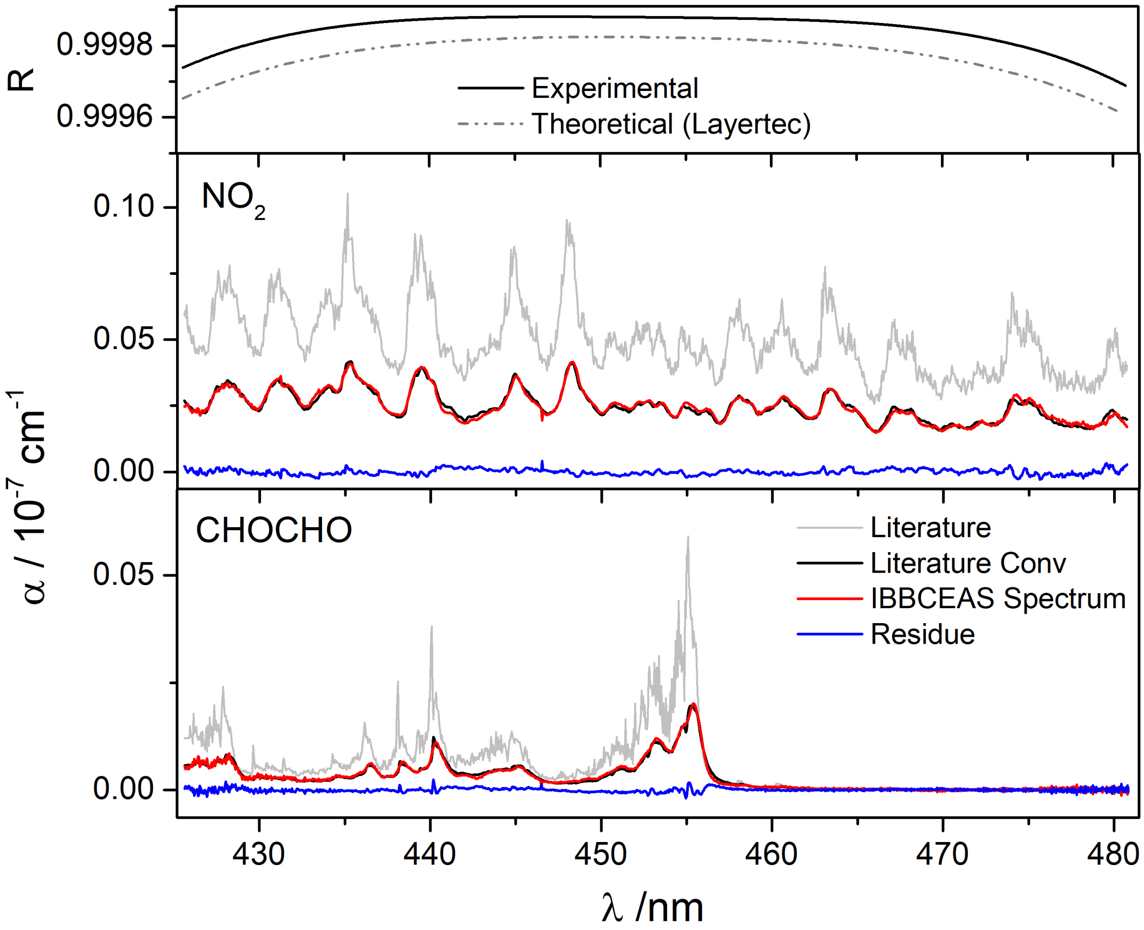

Figure S3. (top) The optimal mirror reflectivity curve (well matching in shape the one provided by the manufacturer) which provides the best match between the literature and experimental spectra. **(middle)** and **(bottom)** The convoluted and unconvoluted literature spectra (Vandaele at al. 1998 for NO_2 and Volkamer et al. 2005 for CHOCHO) and the experimental IBBCEAS spectrum. The blue lines are the residues, i.e. the difference between the experimental and the literature spectra.

S3 Calibration, performance and multi-species detection

S3.1 Long-term stability and instrument sensitivity

The same analysis proposed in the main manuscript for the IBBCEAS-NO_2 are here also reported for the twin IBBCEAS-NO_x instrument. The analysis were done under the same experimental conditions (instrument temperature of 12.0 ± 0.2 °C, cavity pressure of 630.0 ± 0.7 mbar and zero-air flow of 1.07 ± 0.10 L min^{-1}). Similar results on the minimum absorption coefficient and AW statistical analysis were obtained, proving the good reproductibility of those type of sensors (Fig. S4).

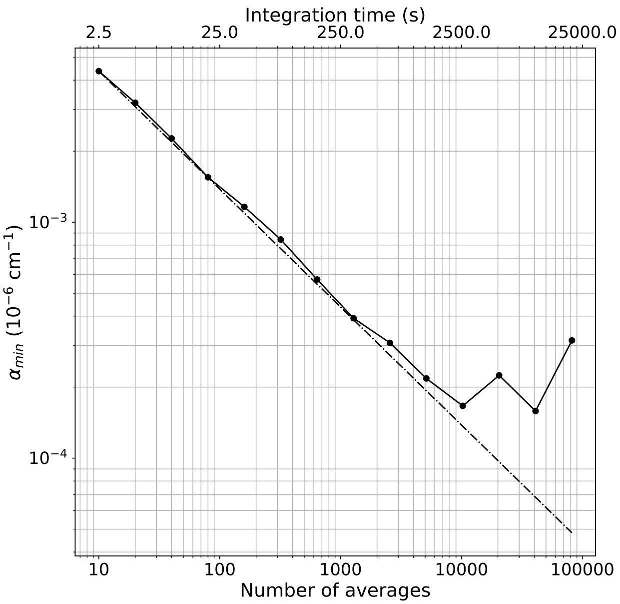

Figure S4. The minimum absorption coefficient $\boldsymbol{\alpha_{min}}$ versus the number of spectral average for the IBBCEAS-NO_x instrument. For these measurements the cell was continuously flushed with a flow of 1.07 L min^{-1} of zero-air, and the $\boldsymbol{\alpha_{min}}$ was calculated from the standard deviation of the residual of the spectra at different time averages.

For 2.5 s acquisition time, corresponding to an average of 10 spectra, the σ_{AW-SD} was 200 ppt for NO_2, 5.6 ppt for IO, 150 ppt for CHOCHO and 800 ppb for O_3. By averaging consecutive spectra, the σ_{AW-SD} decreased following the white noise trend with a characteristic $\sqrt{N}$ slope (where N is the number of spectra). The optimal sensitivity is achieved after 2,600 averages ($\sim$ 11 minutes of measurement for acquiring both the reference and the absorption spectra), where the σ_{AW-SD} reaches 18, 0.42, 12 ppt and 65 ppb for NO_2, IO, CHOCHO and O_3 (1σ), respectively. If the optimum time of measurement is doubled, the system cand achieve ultimate detection limits of 10, 0.32, 9 ppt and 50 ppb for NO_2, IO, CHOCHO and O_3 (1σ), respectively (Fig. S5).

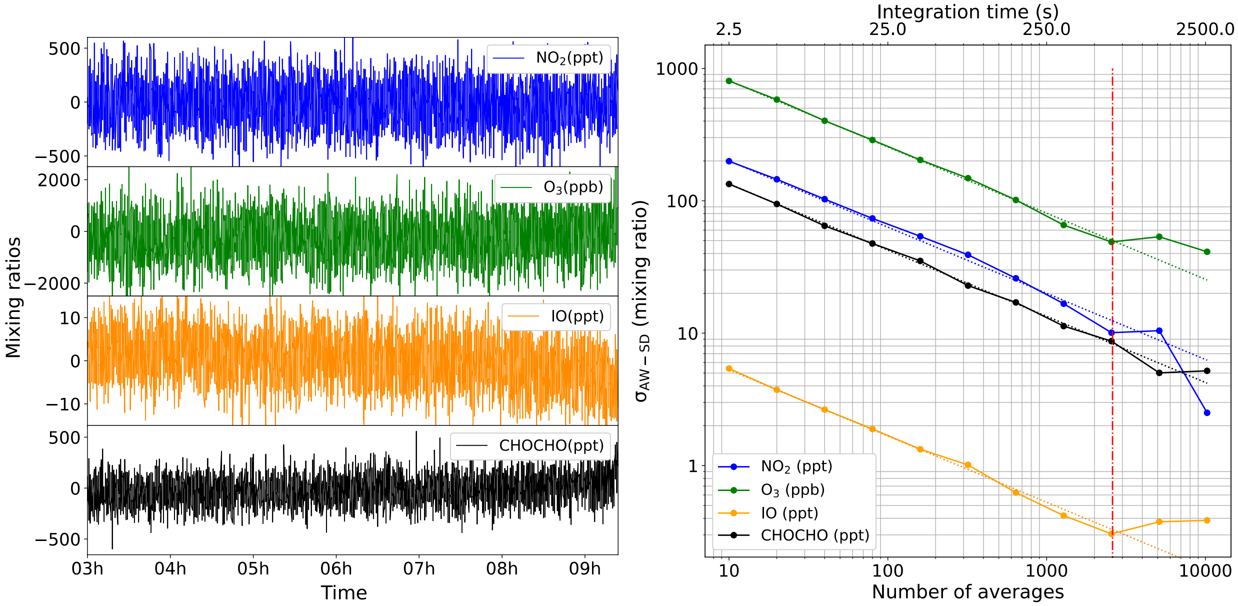

Figure S5. (left) Mixing ratios of the target species NO_2, O_3, IO and CHOCHO, measured during a nine hours Allan-Werle variance statistical experiment flowing zero-air thought the cavity on the IBBCEAS-NO_x instrument. **(right)** The log-log Allan-Werle standard deviation plot, illustrating very similar behavior that for the IBBCEAS-NO_2 instrument reported in the main manuscript.

Fig. S6 shows FIT residuals retrieved using different number of averages (10 - 5,120 - 40,960 and 81,980). The more frequency noise is introduced, the more structures are observed on the residuals. It is therefore a question of finding the right number of averaging operations in order to use the instruments to the best of their respective abilities.

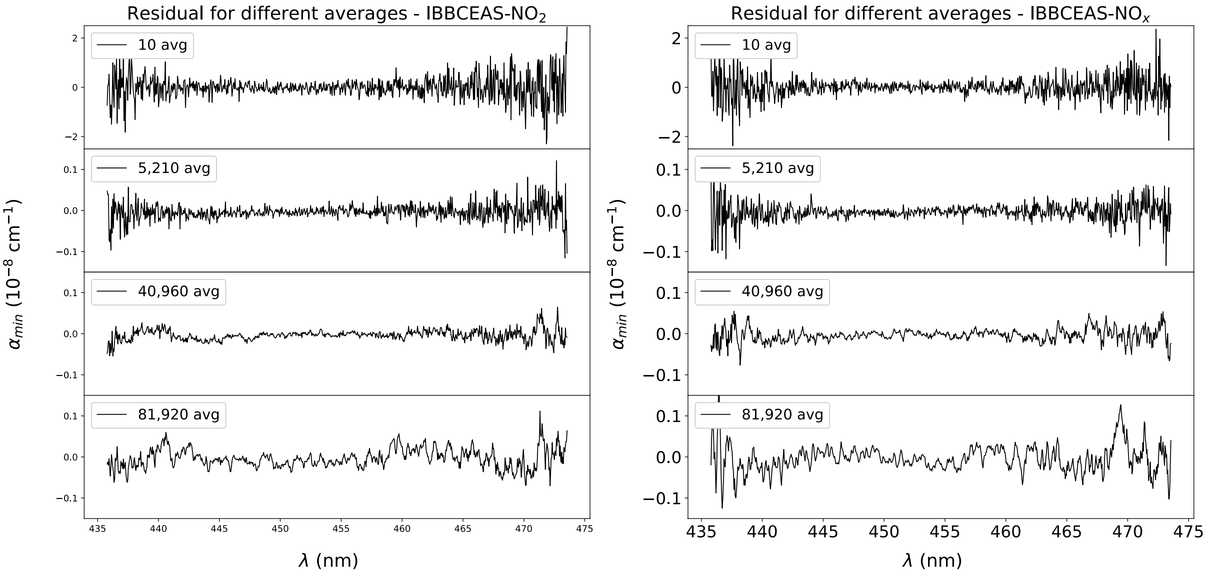

Figure S6. Residuals of the spectral fit at different number of averages for the IBBCEAS-NO_2 **(left)** and IBBCEAS-NO_x instruments **(right)**, showing the arise of structured frequency-dependent noise on the residual of the fit at larger averages.

While the pressure is regulated with a pressure meter with ± 0.2 % accuracy, the cavity's temperature is regulated to be 3 °C above ambient room temperature using a PT100 temperature probe, a temperature controller and heating bands, as described in the manuscript. The heating bands were positioned on the aluminium board which holds all the optics and the cavity. AW analysis were made with and without those heat bands to quantify how sensitive the instruments were to temperature changes, the latter influencing the mechanical stability of the materials. Fig. S7 shows the results obtained with the IBBCEAS-NO_2 instrument. Fig. S7 (left) shows the results without the temperature regulation of the instrument and one can see a deviation from the white noise after 1,300 averages with a maximum at ∼ 10,000 averages or ∼ 42 minutes corresponding to the laboratory temperature regulation cycle. However, by regulating the instrument temperature with the heating bands, the instrument is stable for longer time, and is no longer affected by the external temperature variabilities as shown in Fig. S7 (right) ; similar results were observed for the IBBCEAS-NO_x instrument.

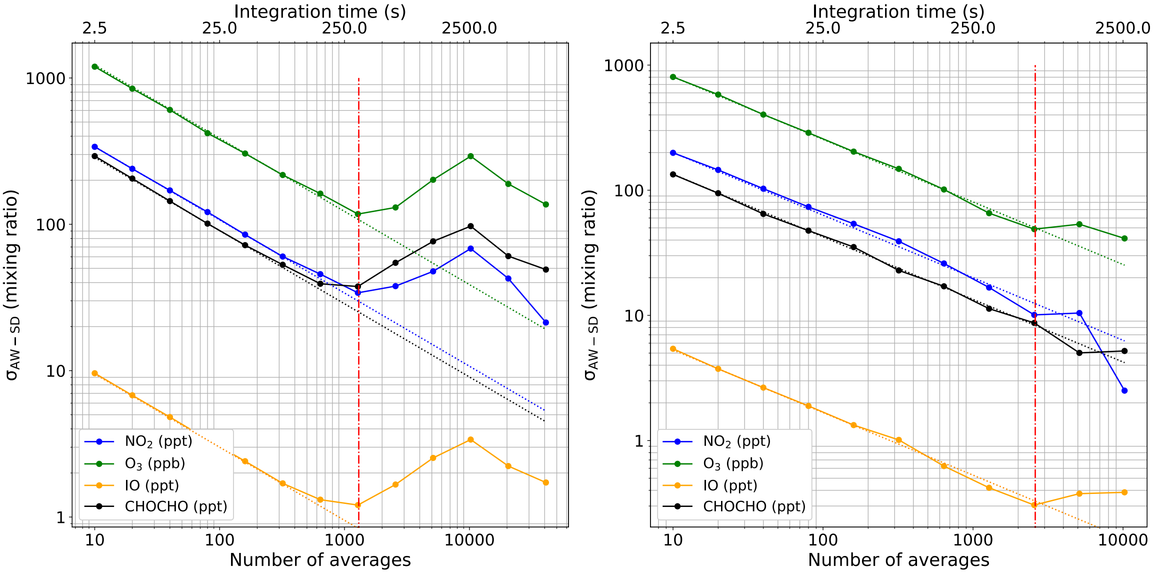

Figure S7. The log-log Allan-Werle standard deviation analysis for the $IBBNO_2$, without **(left)**, and with **(right)**, the temperature regulation of the instrument.

S3.2 Indirect measurement of NO

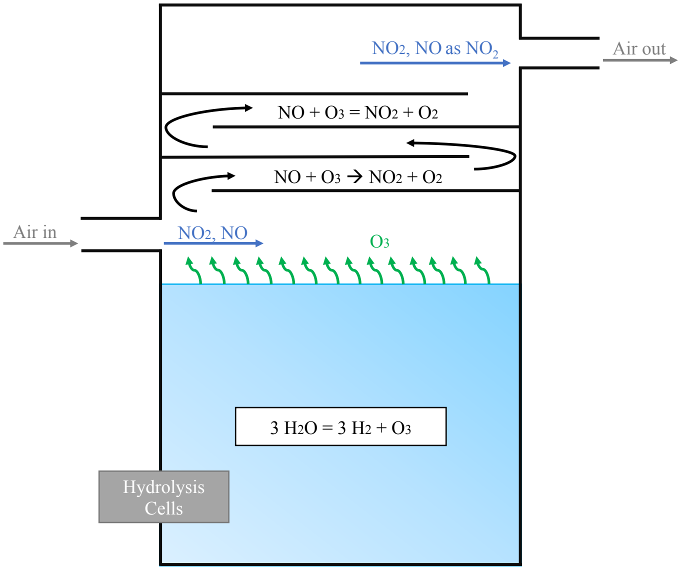

Figure S8. Schematic design of the compact ozone generator. The system sizes is 15 x 15 x 15 cm^3 with a water reservoir of 200 cm^3. A series of electrolytic cells is placed at the bottom, and the air is flushed at the surface before being send to the spectrometer. The cover is designed for enhancing the contact between the water surface and the air as well as preventing water droplets to enter the outlet line.

70 The design of the container, Fig. S8, allows a maximization of the contact area between the air flow and the water and therefore a high ventilation at the surface. The cap was designed with a twisted channel for allowing a better mixing of the gas and preventing water droplet from entering the outlet line.

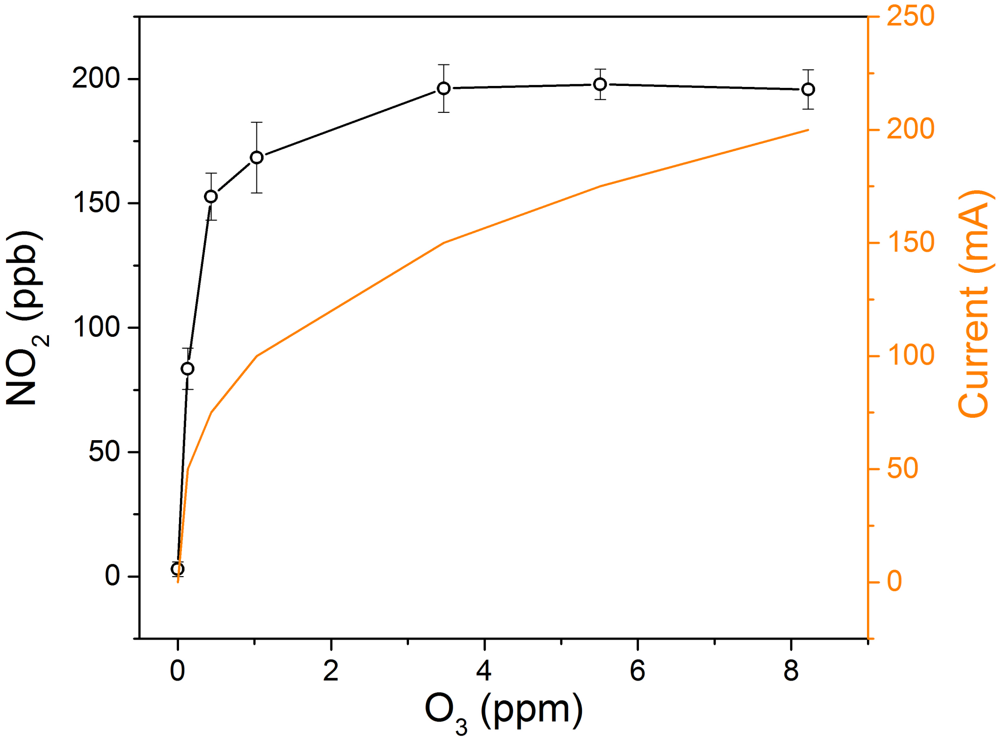

Figure S9. The results from the conversion of NO to NO_2 under ozone excess. The measured NO_2 produced is plotted against the level of O_3 produced by applying a certain current to the sequence of four electrolysis ozone-micro-cells. For the experiment a bottle of $\sim$ 195 ppb of NO in air was used.

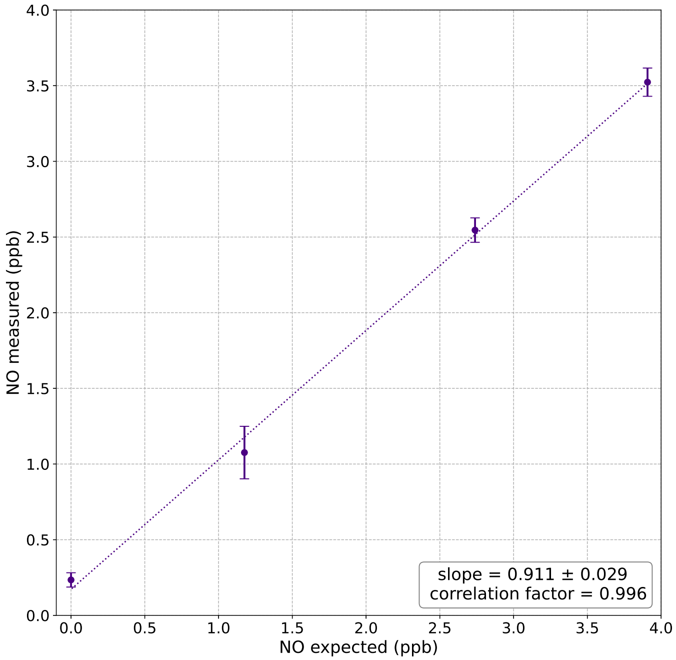

Figure S10. IBBCEAS-NO_x response at different known concentrations of NO (0, 1.1, 2.7 and 3.9 ppb)

The response of the IBBCEAS-NOx instrument was tested by injecting different concentrations of NO (0, 1.1, 2.7 and 3.9 ppb). A NO cylinder from Air Liquide (NO in N_2 at 1 ppm $\pm$ 5 %) was used through a dilution line (Mass Flow Controllers from MKS instrument - ratio of 10,000 : 10) to perform the experiment. The cylinder was previously calibrated with a ThermoFisher™, model 42iTL trace analyzer. The results are shown in Fig. S10 where a linear response with a slope of 0.911 $\pm$ 0.029 and a correlation factor $R^2 = 0.996$ can be observed. The $\sim$ 200 ppt offset read when no NO are expected is due to a left over of NO_2 in the sampling line from a previous NO_2 calibration at high concentrations of NO_2 ($\sim$ 500 ppb), underlining the importance of fluhing the lines with zero air between a calibration and a measurement.